

# Photon pumping, photodissociation and dissipation at interplay for the fluorescence of a molecule in a cavity

M. Gopalakrishna<sup>1</sup>, E. Viñas Boström<sup>2</sup>, C. Verdozzi<sup>3\*</sup>

**1** Department of Physics, Division of Mathematical Physics, Lund University, 22100 Lund, Sweden

**2** Max Planck Institute for the Structure and Dynamics of Matter, Luruper Chaussee 149, 22761 Hamburg, Germany

**3** Department of Physics, Division of Mathematical Physics and ETSF, Lund University, 22100 Lund, Sweden

\* Claudio.Verdozzi@teorfys.lu.se

July 19, 2023

## 1 Abstract

**2** We introduce a model description of a diatomic molecule in an optical cavity,  
**3** with pump and fluorescent fields, and electron and nuclear motion are treated  
**4** on equal footing and exactly. The model accounts for several optical response  
**5** temporal scenarios: a Mollow spectrum hindered by electron correlations, a  
**6** competition of harmonic generation and molecular dissociation, a dependence  
**7** of fluorescence on photon pumping rate, dissipation. It is thus a general and  
**8** flexible template for insight into experiments where quantum photon confine-  
**9** ment, leakage, nuclear motion and electronic correlations are at interplay.

10

---

## 11 Contents

12	<b>1 Introduction</b>	<b>2</b>
13	<b>2 Hamiltonian, initial state and fluorescent spectrum</b>	<b>2</b>
14	2.1 Resonance frequency and fluorescence spectrum	4
15	<b>3 Fluorescence in a rigid molecule and initial state preparation</b>	<b>4</b>
16	3.1 The dependence on the initial conditions	5
17	<b>4 Cavity leakage and atomic motion</b>	<b>6</b>
18	4.1 Nuclear motion	6
19	<b>5 Molecular dissociation and optical response</b>	<b>7</b>
20	<b>6 Conclusion</b>	<b>9</b>
21	<b>A Further details and additional results</b>	<b>9</b>
22	A.1 Resonant frequency for the dimer molecule	9
23	A.2 The interaction parameters	10
24	A.3 Pumping rate and resonant regime for a two-level system	11
25	A.4 Cavity leakage via a Caldeira-Leggett bath: some details	11
26	A.5 Frequency renormalization by the bath(s)	13

## 30 **1 Introduction**

31 Second harmonic generation (SHG) is the conversion by some material system of two pho-  
32 tons of frequency  $\omega$  into a single photon of frequency  $2\omega$ . A classic hallmark of nonlinear  
33 optical behavior [1], SHG still is, sixty years after its discovery [2], the focus of extensive  
34 research in physics [3], engineering [4], chemistry [5], biology [6], and medicine [7]. Part  
35 of this interest stems from technology [8,9]: SHG is the operating mechanism in optical  
36 devices and imaging techniques that are surface or interface sensitive [10–12]. Another  
37 reason is that there are aspects and regimes of SHG still not fully understood, making it  
38 a valuable benchmark for advances in nonlinear optics.

39 Several theoretical methods are used to describe SHG [13], from nonlinear response  
40 in frequency space [14] to Bloch-Maxwell equations [15] and real-time first-principle ap-  
41 proaches [13,16–19]. Often, classical radiation fields are used, which is appropriate in the  
42 strong field limit. However, highly interesting effects in SHG (and fluorescence in general)  
43 appear in the low photon regime [20–23], where quantum effects generally dominate [24]  
44 and the so-called rotating wave approximation (RWA) [25–29] may be inadequate [30–32].

45 Optical cavities permit an accurate selection of confined electromagnetic modes [33–36],  
46 and allow to address the low photon regime of SHG [37]. However, key elements left  
47 out of many theoretical works on few-level systems is an explicit description of electronic  
48 correlations and nuclear dynamics, even though these can importantly affect the harmonic  
49 signal [38–40]. First-principle descriptions include these contributions [13,14,16,19], but  
50 usually approximations are made in numerical implementations. Therefore, because of the  
51 broad relevance of SHG, it is useful to consider model systems where photon pumping,  
52 cavity leakage, electronic correlations, and nuclear motion can be treated exactly and on  
53 equal footing, to gain a generic and accurate understanding of their interplay.

54 In this work we introduce a simple and flexible theoretical framework to describe  
55 a single molecule embedded in an optical cavity, and study its fluorescence properties.  
56 Within this framework all the aforementioned effects and interactions are considered, and  
57 the following picture emerges: (1) the SHG signal is larger for faster photon pumping; (2)  
58 electron-electron interactions strongly reduce the fluorescence signal; (3) for light atomic  
59 masses photodissociation takes place, inhibiting fluorescence and SHG; for heavier masses,  
60 the opposite occurs; (4) both resonant and SHG signals are quenched in time by cavity  
61 leakage. While not tied to any specific molecule, our results unveil a multifaceted light-  
62 matter scenario for SHG and fluorescence in the low photon regime, when multi-photon  
63 effects are important. At the same time, they give qualitative but rigorous initial insight  
64 for more refined investigations of systems of direct experimental interest.

## 65 **2 Hamiltonian, initial state and fluorescent spectrum**

66 We consider a homo-nuclear diatomic molecule embedded in a cavity, where each atom  
67 has a mass  $M$  and a single  $s$ -orbital. The molecule is occupied by two electrons of opposite  
68 spin, interacting with a cavity field of frequency  $\omega_0$  and an fluorescent field of frequency  
69  $\omega$ . The molecule and cavity are assumed to be one-dimensional, with the molecular axis

70 aligned with the axis of the cavity. The total Hamiltonian reads

$$\hat{H}(t) = \hat{H}_s(t) + \hat{V}_{\text{ext}}(t), \quad (1)$$

$$\hat{H}_s(t) = \hat{H}_{\text{mol}} + \hat{H}_{\text{rad}} + \hat{H}_{\text{int}}(t) \quad (2)$$

71 where  $\hat{H}_{\text{mol}}$ ,  $\hat{H}_{\text{rad}}$  and  $\hat{H}_{\text{int}}(t)$  respectively describe the molecule, the photon fields, and  
72 the light-matter interaction [33]. The external field term,  $\hat{V}_{\text{ext}}(t)$ , will be discussed at the  
73 end of this section. In more detail, the molecular Hamiltonian we use is

$$H_{\text{mol}} = \frac{\hat{P}^2}{2(2M)} + \frac{\hat{p}^2}{2(M/2)} + \frac{C}{\hat{x}^4} + U \sum_i \hat{n}_{i\uparrow} \hat{n}_{i\downarrow} - V e^{-\lambda \hat{x}} \sum_{\sigma} (c_{1\sigma}^{\dagger} c_{2\sigma} + c_{2\sigma}^{\dagger} c_{1\sigma}), \quad (3)$$

74 where the first two terms give the kinetic energy of the molecular center of mass (with  
75 momentum  $\hat{P}$ ), and relative atomic motion (with momentum  $\hat{p}$ ). The third term accounts  
76 for an inter-atomic repulsion of strength  $C$ , with  $\hat{x}$  the inter-atomic coordinate. The fourth  
77 term represents an intra-orbital repulsive interaction of strength  $U$  between the electrons,  
78 where  $\hat{n}_{i\sigma} = c_{i\sigma}^{\dagger} c_{i\sigma}$  and  $c_{i\sigma}^{\dagger}$  creates an electron with spin projection  $\sigma$  at atom  $i$ .

79 Finally, the last term in  $\hat{H}_{\text{mol}}$  describes the electron kinetic energy arising from elec-  
80 trons hopping between the atoms. The strength of this contribution is proportional to  
81  $V$ , but it also depends on the internuclear distance via the operator  $e^{-\lambda \hat{x}}$  (with  $\lambda$  an  
82 attenuation parameter). This gives a phenomenological (but intuitively physically plau-  
83 sible [41–44]) fully quantum mechanical interaction between the electrons and the inter-  
84 atomic motion. In the numerical calculations, we set  $V = 2$ ,  $C = 0.6$  and  $\lambda = 0.6$ , to  
85 obtain a Morse-like potential landscape for inter-atomic motion, and an equilibrium po-  
86 sition  $r_0 = 1.156$ . In this way, the effective hopping  $V_{\text{eff}} = V \exp(-\lambda r_0) = 1$  within few  
87 parts per thousand.

88 The second contribution to  $\hat{H}_s$  describes the two photon modes,  $\hat{H}_{\text{rad}} = \omega_0 b^{\dagger} b + \omega b'^{\dagger} b'$ ,  
89 with  $b$  ( $b'$ ) destroying a cavity (fluorescent) photon with frequency  $\omega_0$  ( $\omega$ ). For computa-  
90 tional simplicity we exclude the direct interaction between modes and nuclei, and neglect  
91 center of mass motion [45]. The cavity-molecule interaction is thus  $\hat{H}_{\text{int}} = \hat{\mathcal{M}}[g_c(b^{\dagger} + b) +$   
92  $g'(t)(b'^{\dagger} + b')]$ , where  $\hat{\mathcal{M}} = \sum_{\sigma} (c_{b\sigma}^{\dagger} c_{a\sigma} + c_{a\sigma}^{\dagger} c_{b\sigma})$  and  $c_{b/a} = (c_1 \pm c_2)/\sqrt{2}$  destroys an elec-  
93 tron in the molecule's bonding or antibonding state. In the calculations, the fluorescent  
94 coupling is damped, i.e.  $g'(t) = g_f \exp(-\Gamma t)$  (we set  $\Gamma = 0.02$ ), to describe phenomenolog-  
95 ically cavity losses [22, 37]. Later in the paper, we will supplement this phenomenological  
96 dissipation with a more rigorous description of cavity leakage, by coupling the system to  
97 baths of harmonic oscillators.

98 It useful at this point to briefly comment on these two ways to affect the fluores-  
99 cence response: The phenomenological damping due to  $\Gamma$  acts on the coupling between  
100 the matter and fluorescent photons, to account in an effective way for the fact that the  
101 spontaneous emission into a photon continuum is described via a single effective mode. On  
102 the other hand, with the bath of harmonic oscillators, we describe a dissipation channel  
103 for the photon modes, i.e. for the finite cavity quality. Since the photon-photon coupling  
104 utilised with the harmonic bath can be seen as an effect of all photon modes interacting  
105 via the molecular system, the two effect are clearly related, and yet rather distinct.

106 We will consider two initial light+matter states: i) A product state  $|\Psi_0'\rangle \equiv |g_m\rangle |\beta\rangle_c |0\rangle_f$ ,  
107 with the molecule in its ground state  $|g_m\rangle$  for  $g_c = g_f = 0$ , the cavity field in a coherent  
108 state  $|\beta\rangle_c$ , and the fluorescence field in its vacuum state  $|0\rangle_f$ . ii) The ground state  $|\Psi_0''\rangle \equiv$   
109  $|g\rangle$  of the full Hamiltonian  $\hat{H}_s(t = 0)$ .

110 Lastly, we discuss the external field  $\hat{V}_{\text{ext}}(t)$ . This represents the action of a laser  
111 injecting into the cavity incident photons with frequency  $\omega_0$ . As specified next,  $\hat{V}_{\text{ext}}(t)$   
112 always acts only in the initial part of the simulation interval; in other words,  $\hat{H}(t)$  and

113  $\hat{H}_s(t)$  are time-independent at long times. Explicitly, the form chosen is  $\hat{V}_{\text{ext}}(t) = g_d(b^\dagger +$   
 114  $b)[f(t) \sin \omega_0 t]$ , with a)  $f(t) = \theta(t_s - t)$  a step envelope vanishing after time  $t_s$  or b)  $f(t)$   
 115 a smoothed rectangular pulse. The rectangular pulse  $f(t)$  acts approximately between  
 116  $t_1$  and  $t_2$ , with envelope  $f(t) = [1 - \mathcal{F}_1(t)]\mathcal{F}_2(t)$ , where  $\mathcal{F}_i(t) = [\exp((t - t_i)/\tau_i) + 1]^{-1}$ . In  
 117 all calculations,  $\tau_1 = \tau_2 = 2.0$  whilst the values of  $t_1, t_2$  are case specific, and reported in  
 118 the figure captions.

## 119 2.1 Resonance frequency and fluorescence spectrum

120 We consider a cavity mode with a frequency of either  $\omega_0 = \Omega_R$  in resonance with the  
 121 molecule's electronic transitions, or  $\omega_0 = \Omega_R/2$ . Due to space and spin symmetries,  
 122 the molecule's electronic ground state is a spin singlet of even parity. Since the total  
 123 electron spin  $S$  is conserved in absorption and emission,  $\Omega_R = E_{\text{odd}, S=0}^{\text{ex}} - E_{\text{even}, S=0}^g =$   
 124  $U/2 + [4V_{\text{eff}}^2 + (U/2)^2]^{1/2}$  [46] (see Appendix A.1). Concerning the value chosen for the  
 125 interaction among the electrons, in Appendix A.2 we show that fluorescence weakens on  
 126 increasing the electronic correlations. Accordingly, in the rest of the paper we focus on  
 127 the weakly interacting regime where  $U = 1.0$  and  $\Omega_R = 2.56$ .

128 We characterize the fluorescence spectrum in terms of

$$\mathcal{P}(t, \omega) = \sum_{\lambda r_i n} \sum_{m > 0} |\langle \lambda r_i n m | \mathcal{T} [e^{-i \int_0^t \hat{H}(t') dt'}] | \Psi_0 \rangle|^2, \quad (4)$$

129 where  $\mathcal{P}$  is the probability to have one or more photons in the fluorescence mode  $\omega$  at  
 130 time  $t$  [22]. Here  $|\Psi_0\rangle$  is a given initial state (i.e., either  $|\Psi'_0\rangle$  or  $|\Psi''_0\rangle$  above) and the  
 131  $\omega$ -dependence is contained in  $\hat{H}(t)$ . The sums over  $\lambda$ ,  $r_i$  and  $n$  trace out electronic,  
 132 nuclear and cavity mode degrees of freedom, while the sum over  $m$  ensures that at least  
 133 one fluorescent photon is emitted. The real-time dynamics of the system (with coupled  
 134 electronic, atomic and photonic degrees of freedom) was obtained via the short iterated  
 135 Lanczos algorithm, by computing the exact time evolved many-body state  $|\Psi(t)\rangle$  starting  
 136 from  $|\Psi_0\rangle$ . The configuration size of the problem is  $N = 4N_c N_f N_R$ , where 4 is the  
 137 dimension of the electronic subspace, and  $N_c$ ,  $N_f$ , and  $N_R$  are respectively the maximum  
 138 number of cavity photons, fluorescence photons, and grid points for the nuclear coordinate  
 139  $x$ . We have ensured numerical convergence with respect to these parameters.

## 140 3 Fluorescence in a rigid molecule and initial state prepara- 141 tion

142 In a cavity with low photon number, SHG is remarkably sensitive to the system's initial  
 143 state. This important point is illustrated by comparing the spectra resulting from the  
 144 different initial states  $|\Psi'_0\rangle$  and  $|\Psi''_0\rangle$  introduced earlier. With  $|\Psi'_0\rangle$ , which is a coherent  
 145 state with  $\beta^2$  photons and not an eigenstate of  $\hat{H}_s(t)$ , the system evolves under the full  
 146 Hamiltonian  $\hat{H}_s(t)$  and  $\hat{V}_{\text{ext}} = 0$ . Thus, fluorescence photons are emitted in time. For  
 147  $|\Psi''_0\rangle$ , and with the parameters we consider, the initial occupation of the cavity mode  
 148 is negligible ( $< 10^{-3}$ ). So, for a meaningful comparison with the results from  $|\Psi'_0\rangle$ , the  
 149 cavity is pumped by a driving field  $V_{\text{ext.}}(t)$  of frequency  $\omega_0$ , until an approximately coherent  
 150 state with average photon number  $\langle b^\dagger b \rangle \approx \beta^2$  is reached. The spectra for the two initial  
 151 configurations, and the low photon limit  $\beta = 3$  [47] are in Fig. 1, for both the resonant  
 152 ( $\omega_0 = \Omega_R$ ) and SHG ( $\omega_0 = \Omega_R/2$ ) cases. In the resonant case, and starting from  $|\Psi'_0\rangle$   
 153 (Fig. 1a, empty curves), a spectrum with well-defined Mollow features emerges already  
 154 at early times and converges to a similar profile at longer times. These features can be

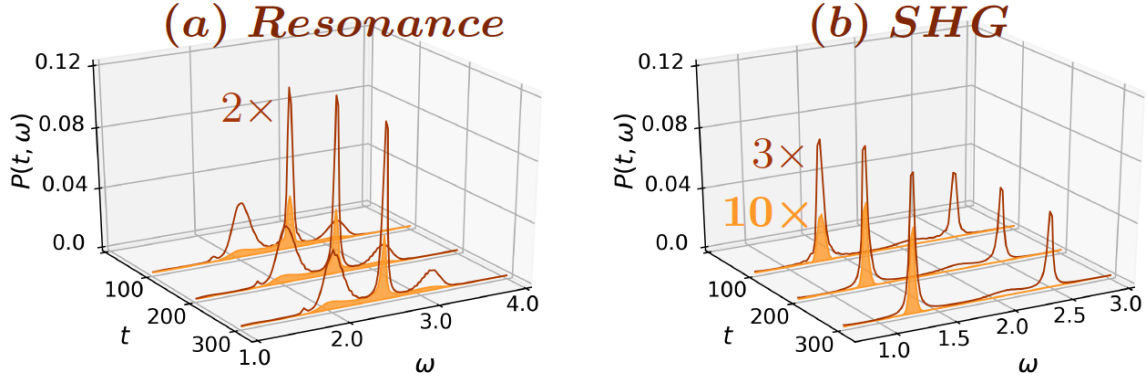


Figure 1: (a) Resonant response for  $\omega_0 = \Omega_R$  and (b) SHG response for  $\omega_0 = \Omega_R/2$  of a rigid molecule, starting from a coherent state  $|\Psi'_0\rangle$  with  $\beta^2 = 9$  (empty curves) and from the cavity+molecule's ground state  $|\Psi''_0\rangle$  followed by pumping (filled curves). For the pumped cavity, the drive is kept on until  $\langle b^\dagger b \rangle \approx 9$ . We use  $t_1 = \frac{6\pi}{\omega_0}$  and  $t_2 = \frac{31\pi}{\omega_0}$ , with  $g_d = 0.229$  and  $0.0996$  in (a) and (b) respectively. In all panels,  $U = 1.0$ ,  $g_c = 0.08$ ,  $g_f = 0.01$ ,  $\Omega_R = 2.56$ , and  $\Gamma = 0.02$ . Plots are scaled for visual clarity and the scaling factors are indicated in color.

155 understood from a dressed-level picture [22,37] since the cavity mode is in resonance with  
 156 a parity allowed transition. Interestingly, starting from  $|\Psi''_0\rangle$  and pumping the cavity up  
 157 to  $\beta = 3$  (Fig. 1a, filled curves), the spectrum at long times is qualitatively similar to  
 158 Fig. 1a empty curves, although the intensity of the Mollow sidebands is reduced compared  
 159 to the main peak. A markedly different picture emerges in the SHG regime: For initial  
 160 state  $|\Psi'_0\rangle$  (Fig. 1b, empty curves), the spectrum quickly develops two sharp features (with  
 161 a broad shoulder in the middle) corresponding to a Rayleigh (SHG) contribution at  $\omega_0$   
 162 ( $2\omega_0$ ). However, when starting from the full ground state  $|\Psi''_0\rangle$  and pumping the cavity,  
 163 the SHG signal is strongly suppressed at all times (Fig. 1b, filled curves). In other words,  
 164 the SHG signal strongly depends on the pumping rate, i.e. on the value of  $g_d$ .

### 165 3.1 The dependence on the initial conditions

166 To uphold our last statement, we consider for simplicity SHG in a two-level system (TLS)  
 167 with levels  $|0\rangle$  and  $|1\rangle$  and  $\omega_0 = \Omega_R/2$ . In Fig. 2a we show the evolution of the total parity  
 168  $\Pi = \langle e^{i\pi b^\dagger b} (\hat{n}_0 - \hat{n}_1) e^{i\pi b^\dagger b} \rangle$ , the cavity mode occupation, and the occupation  $n_1$  of the  
 169 TLS excited state. The dynamics is obtained starting either from a product state with  
 170 the cavity mode in a coherent state (with  $\beta^2 = 1$ ), or from the exact ground state where  
 171 the cavity mode is pumped at different speeds until  $\langle b^\dagger b \rangle \approx 1$ .

172 Fig. 2b shows the corresponding long-time limit SHG. When starting from  $|\Psi'_0\rangle$ ,  $\Pi$  has  
 173 a constant mixed parity  $\Pi_{\text{coh}} \approx 0.17$ . By contrast, when starting from  $|\Psi''_0\rangle$ , initially  $\Pi$  is  
 174 1, but then drops to  $\Pi_{\text{coh}}$  with pumping. Thus, in both cases and at almost all times, the  
 175 system has mixed parity (which is necessary for SHG in a TLS [37]). Yet, the SHG signal  
 176 is absent for slow pumping and very small for fast ramping. Further insight comes from  
 177 how the population  $n_1$  of the excited level changes in time: it is very small for the pumped  
 178 cases, but noticeably larger for the coherent case. Thus, the cavity pumping speed strongly  
 179 affects the population of the excited level and the SHG strength, which increases for faster  
 180 drives, and similar trends are observed for the resonant regime (see Appendix A.3). While  
 181 exemplified for a TLS, our considerations equally hold for the molecule investigated in the  
 182 rest of the paper.

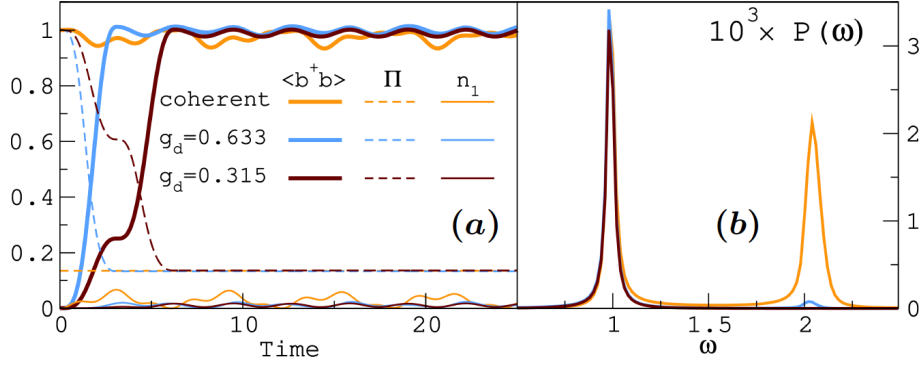


Figure 2: Cavity pumping in a two level system with  $g_c = 0.1, g_f = 0.01, \Gamma = 0.02$ , and  $\omega_0 = \Omega_R/2 = 1$ . Starting from the same ground state, two pumping speeds are considered with  $t_s = \frac{\pi}{\omega_0}$  and  $t_s = \frac{2\pi}{\omega_0}$  respectively. Reference results from an initial coherent state ( $\beta^2 = 1$ ) and no pumping are also shown. (a) Time-evolved average number of cavity photons, total parity and excited state population. (b) Corresponding SHG spectra at long times.

## 183 4 Cavity leakage and atomic motion

184 For a more microscopic treatment of the cavity leakage, we now couple both photon  
 185 modes  $\omega_0, \omega$  to two baths of independent classical oscillators (with variables  $\{x_k, p_k\}$  and  
 186  $\{x'_k, p'_k\}$ ). The couplings of baths and cavity modes are of the Caldeira-Leggett type [48–  
 187 50], and add a contribution  $\hat{H}_{\text{leak}}$  to the system’s Hamiltonian of Eq. (1), with

$$\hat{H}_{\text{leak}} = \frac{1}{2} \sum_{k=1}^{N_B} [(p_k^2 + p'_k{}^2) + \omega_k^2(x_k^2 + x'_k{}^2)] - \sum_{k=1}^{N_B} C_k [x_k(b^\dagger + b) + x'_k(b'^\dagger + b')]. \quad (5)$$

188 In the presence of the baths, the frequency of the modes gets renormalized via  $\omega_0 \rightarrow$   
 189  $\omega_0 + \sum_{k=1}^{N_B} C_k^2/\omega_k^2$  and  $\omega \rightarrow \omega + \sum_{l=1}^{N_B} C_l^2/\omega_l^2$ . Furthermore, an additional “counterterm”  
 190  $\hat{V}_{\text{count.}} \propto [(b^\dagger)^2 + b^2 + (b'^\dagger)^2 + b'^2]$  appears in the Hamiltonian (see Appendix A.4 for  
 191 details), and its role is discussed in Appendix A.5. In the actual calculations,  $\omega_k = k\Delta$   
 192 and  $C_k = A\omega_k^a$ . The values of  $N_B, A, \Delta$  and  $a$  determine the decay rate of the photons  
 193 (the cavity quality). The bath variables are propagated via Ehrenfest dynamics. For  
 194 example, for the  $\{x_k, p_k\}$  bath,  $\ddot{x}_k(t) = -\omega_k^2 x_k(t) + C_k \langle b^\dagger + b \rangle_{\bar{x}, t}$ , where  $\bar{x} \equiv \{x_k\}$ . In turn,  
 195 the coordinates  $\bar{x}, \bar{x}'$  enter parametrically into the wave function  $|\Psi(t)\rangle$  of the quantum  
 196 subsystem (i.e. the cavity modes plus the molecule).

197 Using the Ehrenfest approximation could introduce a problem with detailed balance.  
 198 However, since our approach to cavity leakage does not aim to a quantitative realistic de-  
 199 scription, but rather to explore/illustrate qualitative trends, an incorrect detailed balance  
 200 is not expected to not be a crucial hampering factor. Furthermore, while computationally  
 201 inexpensive, this treatment of the bath keeps the quantum dynamics at the many-body  
 202 wavefunction level unitary and Hermitian.

### 203 4.1 Nuclear motion

204 Until now, the molecule was kept rigid at interatomic distance  $r_0$  corresponding to the  
 205 maximum of  $N(t=0, r)$ , the equilibrium probability distribution of the nuclear relative  
 206 coordinate  $r$ . How the interatomic distance is affected by the light-matter interaction (and  
 207 viceversa) is shown in Fig. 3, where we display time snapshots of  $N(t, r)$  for both resonant



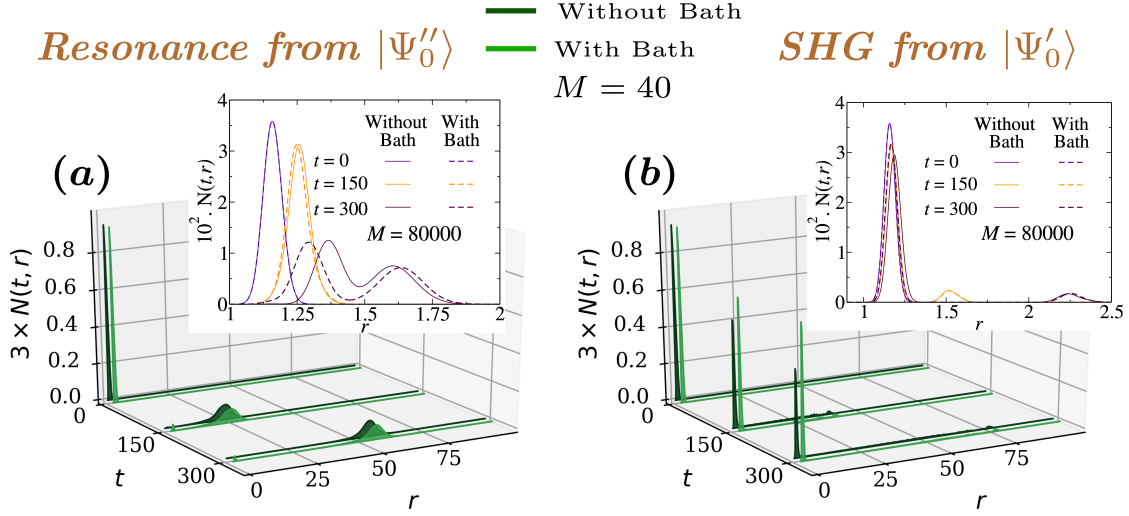


Figure 3: Dynamics of the relative interatomic distance in resonant (a) and SHG (b) regimes, for atomic masses  $M = 40$  (main plots) and  $M = 8 \times 10^4$  (insets). In all panels  $U = 1$  and  $r_0 = 1.156$ . At resonance (a) the calculations were performed by pumping the cavity until  $\langle b^\dagger b \rangle \approx 9$  starting from the interacting ground state  $|\Psi''_0\rangle$ , with  $g_c = 0.03$ ,  $g_f = 0.01$  and  $g_d = 0.151$ . For SHG (b) the calculations started from the product state  $|\Psi'_0\rangle$  with the cavity field in a coherent state with  $\beta^2 = 9$ , with  $g_c = 0.08$ ,  $g_f = 0.01$  and  $\omega_0 = 1.28$ . In all cases displayed, the phenomenological cavity dissipation coefficient  $\Gamma = 0.02$ , either when the baths are included or not. The values of the bath parameters are the same for the incident and the fluorescent fields. They are  $C_k = A(\Delta k)^a$ ,  $N_B = 1000$  oscillators,  $A = 0.005$ ,  $a = 0.6$  and  $\Delta = 0.01$ .

208 and SHG regimes. In these simulations, cavity leakage is included via the oscillator baths,  
 209 whilst other sources of dissipation are still taken into account via an exponential attenu-  
 210 ation ( $g'(t) = g_f e^{-\Gamma t}$ ). In the resonant regime, the system is initially in its ground state  
 211  $|\Psi''_0\rangle$  and the cavity mode is subsequently pumped. In this case, the molecule dissociates  
 212 quite rapidly when  $M = 40$ , irrespective of the presence of the bath. Conversely, for  
 213 the larger mass, no dissociation occurs in the simulation interval, and the atoms remain  
 214 around the equilibrium configuration with a broadened distribution  $N(t, r)$ .

215 In the SHG regime, the system's initial state is  $|\Psi'_0\rangle$  for both values of  $M$ . Here,  
 216 the molecule predominantly remains close to the equilibrium configuration at all times,  
 217 especially when leakage is added. That is, the tendency to delocalise is greater when only  
 218 the exponential damping is present, indicating that cavity leakage also plays a role. As  
 219 shown next, the different atomic dynamics affect the optical response in distinct ways.

## 220 5 Molecular dissociation and optical response

221 Fig. 4 shows the fluorescence spectra for finite  $M$ , with all the elements previously dis-  
 222 cussed (photon pumping speed, atomic dynamics and cavity leakage) at interplay. The  
 223 spectra in panels (a,b) and (c,d) respectively correspond to the atomic probabilities  $N(t, r)$   
 224 of Fig. 3a and Fig. 3b. At resonance, the fluorescence spectrum strongly depends on the  
 225 value of the atomic mass: For  $M = 40$  the molecule dissociates (see Fig. 3a) and  $\mathcal{P}(t, \omega)$   
 226 exhibits sharp features as well as a plateau, in stark difference to the Mollow-like structure  
 227 of the rigid molecule limit. Conversely, for  $M = 8 \times 10^4$ , the molecule remains localized

Resonant:  $|\Psi_0''\rangle$  at  $t = 0$ , pumping at  $t > 0$

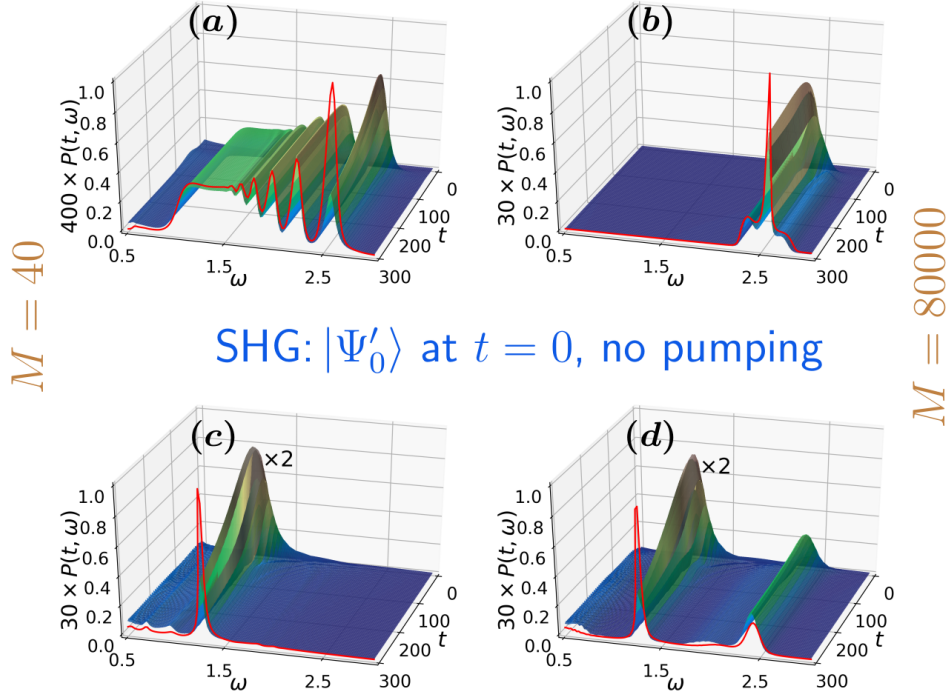


Figure 4: Time-dependent fluorescence for atomic masses  $M = 40$  (a, c) and  $M = 8 \times 10^4$  (b, d). The time evolution was performed with the classical baths, whilst the red curves show the long-time limit of  $\mathcal{P}(t, \omega)$  in the absence of leakage. The bath parameters are the same for the bath of the incident field and the one of the fluorescent field. They are  $N_B = 1000$  oscillators, with  $C_k = A(\Delta k)^a$ ,  $A = 0.005$ ,  $a = 0.6$  and  $\Delta = 0.01$ . In all the calculations  $\Gamma = 0.02$ . (a, b) Resonant case, starting from  $|\Psi_0''\rangle$  and pumping the cavity until  $\langle b^\dagger b \rangle \approx 9$ ,  $t_1 = \frac{6\pi}{\omega_0}$ ,  $t_2 = \frac{41\pi}{\omega_0}$ ,  $g_d = 0.151$ ,  $g_c = 0.03$ ,  $g_f = 0.01$  and  $\omega_0 = 2.56$ . (c, d) SHG case, starting from  $|\Psi_0'\rangle$  with  $\beta^2 = 9$ ,  $g_c = 0.08$ ,  $g_f = 0.01$  and  $\omega_0 = 1.28$ . The time-evolved plots are magnified for visual clarity, and in all cases  $U = 1$  and  $r_0 = 1.156$ .

228 around the equilibrium position (inset in Fig. 3a), and at long times  $\mathcal{P}(t, \omega)$  is peaked  
 229 around the resonant value ( $\Omega_R = 2.56$ ). Overall, the shape of  $\mathcal{P}(t, \omega)$  with or without the  
 230 bath dissipation show a mutual resemblance at long times. However, for bath dissipation  
 231 the intensity of  $\mathcal{P}(t, \omega)$  is considerably weaker.

232 A quite different picture emerges for SHG regime (Fig. 4c and d), where  $\mathcal{P}(t, \omega)$  is  
 233 considerably weaker in the case of an oscillator bath. Also, when the molecule dissoci-  
 234 ates (Fig. 4c), the SHG signal is absent irrespective of the presence or not of the baths.  
 235 Conversely, for larger  $M$ , the SHG signal is present if the system evolves in contact with  
 236 an oscillator bath, but with smaller intensity. This suggests that the multi-photon cavity  
 237 field is much more affected by dissipation under off-resonant conditions than at resonance.

238 In summary, in the dissociation regime both resonant Mollow and SHG signals are  
 239 quenched. Also, for dissipation via an oscillator bath, for a broad range of atomic mass  
 240 values fluorescence is always vastly reduced. Finally, even with no cavity leakage, the  
 241 strength of the SHG response is determined by the cavity pumping rate.



## 242 6 Conclusion

243 Many decades of nonlinear optics research gave us a robust conceptual understanding of  
 244 SHG, and actual uses in technology. Yet, some SHG regimes remain little explored, and  
 245 how different physical mechanisms and interactions contribute to fluorescence is not always  
 246 understood. In this work, we studied theoretically one of these (namely, the low photon)  
 247 regimes, using a model molecule in an optical cavity, and via an exact time-dependent con-  
 248 figuration interaction (TDCI) approach, where all quantum degrees of freedom (electrons,  
 249 photons and relative atomic motion) are included on equal footing and supplemented by  
 250 a semi-classical treatment of cavity dissipation/leakage.

251 Our study reveals a previously unknown, complex landscape for fluorescence, where the  
 252 latter is reduced by electronic interactions and by cavity leakage, enhanced by fast cavity  
 253 pumping, and quenched by molecular photodissociation. These competing trends likely  
 254 occur in real molecules as well; it should thus be possible to detect them in experiments  
 255 at low photon regimes. Our theoretical and computational framework can be applied and  
 256 extended in different ways, e.g. more realistic molecules, or cavities with more than one  
 257 molecule. Other possibilities are few ultracold bosons in cavities, to provide insight for  
 258 SHG in the Gross-Pitaevskii limit [51], or fermions in the (interacting) Dicke’s model, in  
 259 conjunction with other techniques that exhibit better size-scaling behavior than TDCI,  
 260 e.g. nonequilibrium Green’s functions [52]. Some of these undertakings are under way.

## 261 Acknowledgements

262 We acknowledge A. D’Andrea for discussions.

263 **Author contributions** M.G. performed all calculations and interpretation of results  
 264 under the supervision of E.V.B. and C.V. The project was conceived by E.V.B. and C.V.  
 265 The overall supervision of the project was by C.V. Both M.G. and E.V.B. contributed to  
 266 the writing of the code. All authors collaborated in writing the paper.

267 **Funding information** M.G. and C.V. acknowledge support from the Swedish Research  
 268 Council (grant number 2017-03945).

## 269 A Further details and additional results

### 270 A.1 Resonant frequency for the dimer molecule

271 To discuss the selection rules for light absorption, it suffices to consider a fixed molecule.  
 272 The relevant part of the molecule Hamiltonian in this case is

$$H_e = -V_{eff}^{eq} \sum_{\sigma} (\hat{c}_{1\sigma}^{\dagger} \hat{c}_{2\sigma} + \hat{c}_{2\sigma}^{\dagger} \hat{c}_{1\sigma}) + U \sum_{i=1,2} \hat{n}_{i+} \hat{n}_{i-}, \quad (6)$$

273 where  $V_{eff}^{eq} > 0$ . The molecule-light interaction for the two cavity modes is taken as  
 274  $\hat{H}_{int}(t) = \hat{\mathcal{M}} [g_c(b^{\dagger} + b) + g'(t)(b'^{\dagger} + b')]$ , where  $\hat{\mathcal{M}} = \sum_{\sigma} (c_{b\sigma}^{\dagger} c_{a\sigma} + c_{a\sigma}^{\dagger} c_{b\sigma})$ . For two electrons  
 275 of opposite spin,  $H_e$  has three singlet eigenstates ( $S = S_z = 0$ ) and one triplet eigenstate  
 276 ( $S = 1, S_z = 0$ ). The eigenvalues are 0 for  $S = 1$  and  $U, U/2 \mp \sqrt{4(V_{eff}^{eq})^2 + (U/2)^2}$  for  
 277  $S = 0$ . The ground state is the singlet with energy  $U/2 - \sqrt{4(V_{eff}^{eq})^2 + (U/2)^2}$ , and it is

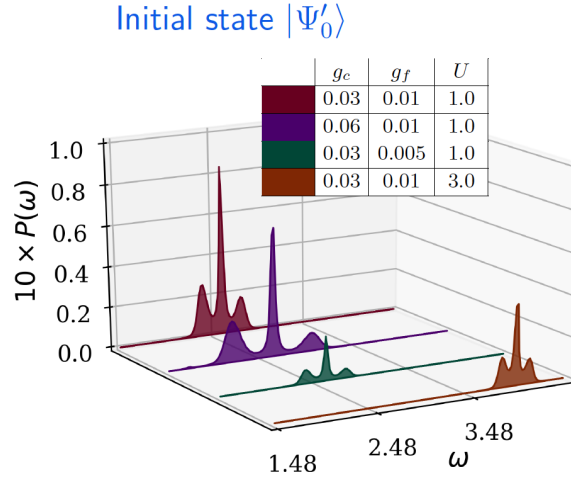


Figure 5: Fluorescent spectra for the rigid molecule starting with a coherent state with  $\beta = 3$ ,  $r_0 = 1.156$ ,  $\Gamma = 0.02$ ,  $\Omega_R = 2.56$  and  $\omega_0 = \Omega_R$ . Only for the  $U = 3.0$  case, it is  $\Omega_R = \omega_0 = 3.95$  and  $r_0 = 1.213$ .

278 even under spatial parity. The eigenstates with odd symmetry under parity have energies  
 279 0 with  $S = 0$  and  $U$  with  $S = 1$ .

280 It can be easily shown that optical transitions between the two even ( $E$ ) many-body  
 281 states or between the two odd ( $O$ ) many-body states are forbidden (e.g.  $\langle E_1 | \hat{\mathcal{M}} | E_2 \rangle = 0$ ),  
 282 and the only permitted transitions are between odd and even ones (i.e. with opposite  
 283 parity). Furthermore, using the matrix expressions above for  $\hat{\mathcal{M}}$  and  $\hat{\mathbf{S}}^2$ , one can show  
 284 that  $[\hat{\mathcal{M}}, \hat{\mathbf{S}}^2] = 0$ . So the only transition allowed from the ground state is the even-odd one  
 285 where the system goes  $|g, S = 0\rangle \rightarrow |O, S = 0\rangle$  and where the energy difference is  $\Omega_R =$   
 286  $E_{O,S=0} - E_{g,S=0} = U/2 + \sqrt{4(V_{eff}^{eq})^2 + (U/2)^2}$ , which defines the “many-body” resonance  
 287 condition for the  $\omega_0$  field in perturbation theory, similar to the two-level single-particle  
 288 case. More in general, for the multi-photon case of interest here, the bare electronic many-  
 289 body levels are renormalised by the photons, parity gets mixed up, and more transitions  
 290 are possible and, most importantly, the parity of the full electron+photon systems must  
 291 be considered. In the presence of nuclear dynamics, the values of the effective hopping  
 292 parameter in the dimer changes in time and so it does  $\Omega_R$ .

## 293 A.2 The interaction parameters

294 Before choosing the values for the parameters  $g_c$ ,  $g_f$  and  $U$  used in the paper, we have  
 295 performed calculations to observe their effect on the spectra. A sample of the ensuing  
 296 results is reported in Fig. 5. Due to coupling between light and the molecule, the molecular  
 297 levels will split and the splitting energy is  $\propto g_c$  [37]. Hence the regime of the emitted  
 298 photon frequency will be affected by the incident field coupling, as observed in Fig. 5.  
 299 On increasing  $g_c$ , the fluorescent spectra get broadened, since this involves large range  
 300 of frequencies for the emitted photon. On the other hand, Increasing the coupling  $g_f$   
 301 increases the intensity of the fluorescent spectra. The electron interaction  $U$  hinders  
 302 electronic hopping between the two sites of the molecule. The emission of the fluorescent  
 303 photon requires a transition among bonding and the anti-bonding molecular levels, and  
 304 thus it involves electron hopping between the molecular sites. Accordingly, increasing the  
 305 electron interaction decreases the intensity of the emitted photon, as it can be observed  
 306 in Fig. 5.

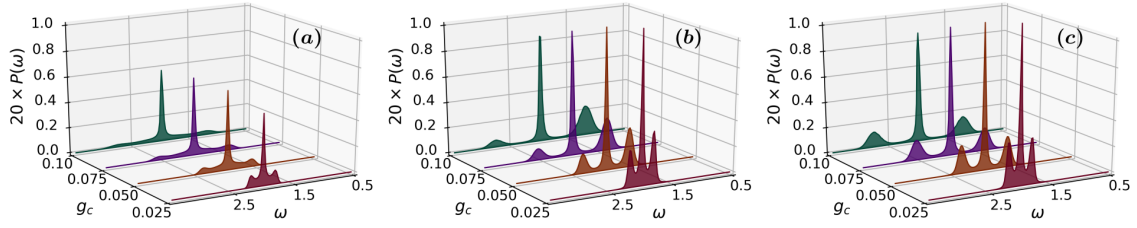


Figure 6: Long-time limit of fluorescence spectra for a two-level system in the resonant regime and in a pumped cavity with  $g_d = 0.232$ ,  $t_1 = \frac{6\pi}{\omega_0}$ ,  $t_2 = \frac{31\pi}{\omega_0}$ , (a) and  $g_d = 5.150$ ,  $t_s = \frac{\pi}{\omega_0}$  (b). The pumping is applied until  $\langle b^\dagger b \rangle \approx 16.0$  in the cavity and the initial state is  $|\Psi_0'\rangle$ . Reference results starting the time evolution from an initial coherent  $|\Psi_0'\rangle$  state with  $\langle b^\dagger b \rangle = 16.0$  but without pumping are also shown (c). Spectral intensities are in arbitrary units, and parameters common to all panels are  $g_f = 0.01$ ,  $\Gamma = 0.02$  and  $\omega_0 = \Omega_R = 2.0$ .

### 307 A.3 Pumping rate and resonant regime for a two-level system

308 In Fig. 6, we show  $\mathcal{P}(\omega)$  for  $\omega_0 = \Omega_R$  for two driving speeds as well as for photons initially  
 309 in a coherent state. We observe similar trends as in the SHG regime discussed in Fig. 2,  
 310 namely fast pumping leads to closer agreement with the coherent state spectrum. Since  
 311 photons interact with the TLS during the drive, the coherent and fast-drive spectra become  
 312 increasingly similar when the system-cavity interaction  $g_c$  is decreased.

### 313 A.4 Cavity leakage via a Caldeira-Leggett bath: some details

314 To introduce leakage in the cavity, we use ideas borrowed from the physics associated with  
 315 the Caldeira-Leggett model (CLM). As specified in Eq. (5) of the main text, we connect  
 316 each the two modes  $\omega_0$  and  $\omega$  to a bath of  $N_B$  classical oscillators. In the following,  
 317 however, to provide details about the procedure, we consider for simplicity only one mode,  
 318 say the  $\omega_0$  incident mode. The case of the second (fluorescent) mode can be treated  
 319 similarly.

320 The classical version of the CLM is defined as

$$H = \frac{\tilde{p}^2}{2\mu} + V(x) + \sum_{k=1}^{N_B} \left[ \frac{p_k^2}{2m_k} + \frac{1}{2} m_k \omega_k^2 \left( x_k - \frac{C_k}{m_k \omega_k^2} x \right)^2 \right], \quad (7)$$

321 where  $\tilde{p}^2/2\mu + V(x)$  is the system (particle) Hamiltonian and the bath degrees of freedom  
 322 are represented by the  $2N_B$ -tuple  $\{x_k, p_k\}$ . The oscillators have masses and frequencies  
 323  $\{m_k, \omega_k\}$ , and the coefficient  $\{C_k\}$  determine the interaction between the particle and  
 324 the bath. The form of the interaction term is chosen in this way to ensure translational  
 325 invariance of the model in some specific situations [48]. The solution of Eq. (7) can be  
 326 written as

$$\mu \ddot{x}(t) + \frac{dV}{dx} + \mu \int_{t_0}^t \gamma(t-t') \dot{x}(t') dt' = -\mu \gamma(t-t_0) x(t_0) + F_L(t), \quad (8)$$

327 where  $\gamma(t)$  determines the dissipative features of the bath (for example, for  $\gamma(t) \rightarrow \gamma_0 \delta(t)$ ,  
 328 we have a standard friction term), and  $F_L(t)$  is a noise-like, oscillating force coming from  
 329 the bath degrees of freedom. In the continuum-bath limit,  $\gamma$  takes the form

$$\gamma(t) = \frac{2}{\pi} \int \frac{J(\omega)}{\mu \omega} \cos \omega t \, d\omega, \quad (9)$$

330 where  $J(\omega) = \frac{\pi}{2} \sum_{k=1}^{N_B} \frac{C_k^2}{m_k \omega_k} \delta(\omega - \omega_k)$  is the spectral density of the bath (here, and in the  
 331 rest of this section,  $\omega$  is the variable Fourier-conjugated to  $t$ ). Often, in practice, one takes  
 332  $J(\omega) \propto \omega^\alpha$  in an interval range  $[0, \omega_c]$ , and zero otherwise. To describe the leaking from  
 333 the cavity modes, we adopt a modified form of the CLM, where the cavity modes are in  
 334 the second quantisation picture, the masses  $\mu = m_k = 1$ , and we neglect the zero energy  
 335 of the cavity mode. Specialising to the mode  $\omega_0$ , this gives

$$\begin{aligned}
 \hat{H}_{1mode}(t) = & (\omega_0 + \sum_{k=1}^{N_B} \frac{C_k^2}{\omega_k^2}) b^\dagger b + \sum_{k=1}^{N_B} (\frac{p_k^2}{2} + \frac{1}{2} \omega_k^2 x_k^2) - \sum_{k=1}^{N_B} C_k x_k (b^\dagger + b) + \left[ \sum_{k=1}^{N_B} \frac{C_k^2}{\omega_k^2} \right] \frac{(b^\dagger)^2 + b^2}{2} \\
 & + \hat{H}_{mol} + V_{ext}(t) + \hat{M} g_c (b^\dagger + b), \quad (10)
 \end{aligned}$$

336 where  $\hat{M}$  describes the electronic transitions. In this case, with  $\tilde{C}_k = (2\omega_0)^{\frac{1}{2}} C_k$ , we have  
 337  $J(\omega) = \frac{\pi}{2} \sum_{k=1}^{N_B} \frac{\tilde{C}_k^2 \delta(\omega - \omega_k)}{m_k \omega_k}$ . To choose the set  $\{\tilde{C}_k\}$ , we consider that, for a very large  
 338 frequency  $\omega_{Max}$ , we get  $\int_0^{\omega_{Max}} J(\omega) d\omega = \sum_{k=1}^{N_B} \frac{\tilde{C}_k^2}{\omega_k}$ . By approximating the integral with a  
 339 discrete sum with frequency step  $\Delta$ ,

$$\sum_{k=1}^{N_B} \frac{\tilde{C}_k^2}{\omega_k} = \int_0^{\omega_{Max}} J(\omega) d\omega \approx \sum_{k=1}^{N_B} J(\omega_k) \Delta \quad (11)$$

340 and thus  $\frac{\tilde{C}_k^2}{\omega_k} \approx J(\omega_k) \Delta$ . In turn, this amounts to say that [48, 49]

$$\frac{C_k^2}{\omega_k} (2\omega) \approx J(\omega_k) \Delta \Rightarrow C_k \approx \sqrt{J(\omega_k) \omega_k}. \quad (12)$$

341 The actual dynamics is performed according to the quantum-classical (Ehrenfest's) approx-  
 342 imation, where the molecule+boson (m+b) system is quantum and the bath is classical.  
 343 The equations of motion then are:

$$i \frac{d|\psi_{m+b}(t)\rangle}{dt} = \tilde{H}(\{x_k(t)\}) |\psi_{m+b}(t)\rangle, \quad (13)$$

$$\ddot{x}_k(t) = -\omega_k^2 x_k(t) + C_k(t) \langle b^\dagger + b \rangle_t, \quad (14)$$

$$\dot{x}_k = p_k \quad (15)$$

344 where

$$\begin{aligned}
 \tilde{H}(\{x_k(t)\}, t) = & (\omega_0 + \sum_{k=1}^{N_B} \frac{C_k^2}{\omega_k^2}) b^\dagger b - (b^\dagger + b) \sum_{k=1}^{N_B} C_k x_k(t) + \left[ \sum_{k=1}^{N_B} \frac{C_k^2}{\omega_k^2} \right] \frac{(b^\dagger)^2 + b^2}{2} \\
 & + \hat{H}_{mol} + V_{ext}(t) + \hat{M} g_c (b^\dagger + b) \quad (16)
 \end{aligned}$$

345 The bosonic Schrödinger equation is solved as usual while for the bath fields we use the  
 346 coordinate Verlet algorithm. In the actual calculations, the parameters were chosen such  
 347 as  $\omega_k = \Delta k$  and  $C_k \propto k^a$ . As it can be gathered from the foregoing discussion, the case  
 348 of the fluorescent field in the presence of a bath can be treated similarly. The system of  
 349 equations for the full system thus is

$$i \frac{d|\psi_{m+b}(t)\rangle}{dt} = \tilde{H}(\{x_k(t)\}, \{x'_l(t)\}, t) |\psi_{m+b}(t)\rangle, \quad (17)$$

$$\ddot{x}_k(t) = -\omega_k^2 x_k(t) + C_k(t) \langle b^\dagger + b \rangle_t, \quad \dot{x}_k = p_k \quad (18)$$

$$\ddot{x}'_l(t) = -\omega_l^2 x'_l(t) + C_l(t) \langle b^\dagger + b' \rangle_t, \quad \dot{x}'_l = p'_l \quad (19)$$

350 where

$$\begin{aligned}
 \tilde{H}(\{x_k(t)\}, \{x'_l(t)\}, t) &= \tag{20} \\
 &= (\omega_0 + \sum_{k=1}^{N_B} \frac{C_k^2}{\omega_k^2}) b^\dagger b - (b^\dagger + b) \sum_{k=1}^{N_B} C_k x_k(t) + \left[ \sum_{k=1}^{N_B} \frac{C_k^2}{\omega_k^2} \right] \frac{(b^\dagger)^2 + b^2}{2} \\
 &+ (\omega_0 + \sum_{l=1}^{N_B} \frac{C_l^2}{\omega_l^2}) b^\dagger b' - (b^\dagger + b') \sum_{l=1}^{N_B} C_l x'_l(t) + \left[ \sum_{l=1}^{N_B} \frac{C_l^2}{\omega_l^2} \right] \frac{(b^\dagger)^2 + b'^2}{2} \\
 &+ \hat{H}_{\text{mol}} + V_{\text{ext}}(t) + \hat{\mathcal{M}}[g_c(b^\dagger + b) + g'(t)(b^\dagger + b')].
 \end{aligned}$$

351

352

### 353 A.5 Frequency renormalization by the bath(s)

354 As seen in Appendix A.4, in the presence of baths the frequencies  $\omega_0, \omega$  become renormal-  
 355 ized, and an additional interaction contribution of the kind  $(b^\dagger)^2 + b^2$  appears. The origin  
 356 of these changes is easily understood looking at the classical CLM in Eq. (7): they are  
 357 due to the contribution  $\frac{1}{2} \sum_k \frac{C_k^2}{m_k \omega_k^2} x^2$ , that in the quantum case behaves like  $\approx (b^\dagger + b)^2$ .  
 358 As mentioned earlier, such term is present to ensure that the particle-bath interaction  
 359 is translationally invariant, e.g. when  $C_k = m_k \omega_k^2$  or when a coordinate transformation  
 360 is performed. However, for the system considered here, this is a *non issue*: a (finite)  
 361 cavity breaks translational invariance. However, since it is customary in the literature to  
 362 consider the CLM as in Eq. (7), we wish to discuss here the role of this changes for our  
 363 molecule+cavity system. Similarly to Appendix A.4, we will carry out our analysis in  
 364 terms of the  $\omega_0$  mode only.

365 Let us to write again  $H_{1mode}$  from Eq. (10), but more concisely:

$$\hat{H}_{1mode}(t) = (\omega_0 + A) b^\dagger b + A \frac{(b^\dagger)^2 + b^2}{2} \tag{21}$$

$$+ \hat{\mathcal{M}} g_c(b^\dagger + b) - \sum_{k=1}^{N_B} C_k x_k(b^\dagger + b) + \hat{H}_{\text{mol}} + \hat{H}_{\text{bath}} + V_{\text{ext}}(t) \tag{22}$$

366 where  $A = \sum_k \frac{C_k^2}{\omega_k^2}$ , and  $H_{\text{bath}} = \sum_{k=1}^{N_B} (\frac{p_k^2}{2} + \frac{1}{2} \omega_k^2 x_k^2)$ . Clearly, setting  $A = 0$  in this  
 367 expression is an approximation (it forces the removal of the quadratic terms). We also  
 368 wish at this point to make explicit the form external potential:

$$V_{\text{ext}}(t) = g_d f(t) \sin(\omega'' t) (b^\dagger + b) \equiv g_d^{\omega''}(t) (b^\dagger + b). \tag{23}$$

369 This is the same as in the paper, but with the notable difference that the frequency  $\omega''$   
 370 is left unspecified (in the paper,  $\omega' = \omega_0$  always). We can now proceed to a Bogolubov  
 371 transformation  $\begin{pmatrix} b \\ b^\dagger \end{pmatrix} = \begin{pmatrix} u & v \\ v & u \end{pmatrix} \begin{pmatrix} d \\ d^\dagger \end{pmatrix}$  of the terms of the first line of Eq. 22, and  
 372 rewrite

$$(\omega_0 + A) b^\dagger b + (A/2)[(b^\dagger)^2 + b^2] \rightarrow \Omega d^\dagger d, \quad \text{where } u/v = [\sqrt{\omega_0/\Omega} +/ - \sqrt{\Omega/\omega_0}]/2,$$

373 and  $\Omega = (\omega_0^2 + 2\omega_0 A)^{\frac{1}{2}}$ . Extending the transformation to the other terms of  $\hat{H}_{1mode}$ , we  
 374 finally arrive at

$$\hat{H}_{1mode} = \Omega d^\dagger d + \sqrt{\frac{\omega_0}{\Omega}} \left[ g_c \hat{\mathcal{M}} - \sum_{k=1}^{N_B} C_k x_k + g_d^{\omega''}(t) \right] (d^\dagger + d) + \hat{H}_{\text{mol}} + \hat{H}_{\text{bath}}, \tag{24}$$

375 where we used Eq. (23) for  $V_{\text{ext}}(t)$ , and where some constant term have been dropped. As  
376 shown in Appendix A.4 in a related context, the manipulations done here apply straight-  
377 forwardly to the fluorescent mode.

378 As a final point, and specifically considering the incident mode, we observe that if in  
379 Eq. (24) we set  $\omega'' = \omega_0$ , we then go back to the slightly-off-resonance case studied in the  
380 paper, but described in another, exact, representation (we have verified numerically that  
381 this is the case).

382 However, if we imagine that  $V_{\text{ext}}(t)$  describes a laser with a tuneable frequency, we see  
383 that at  $\omega'' = \Omega$ , we are again in resonance with a cavity with an effective frequency  
384 renormalised by the bath(s), which should reflect as usual into an enhancement of the sig-  
385 nal. Quite interestingly, both at- and away-from-resonance the problem can be described  
386 with a CLM bath without a quadratic term in  $(d^\dagger + d)^2$ , i.e. the translational invariance  
387 requirement does not play explicitly a role.

## 388 References

- 389 [1] N. Bloembergen and P.S. Pershan, *Light Waves at the Boundary of Nonlinear Media*,  
390 Phys. Rev. **128**, 606 (1962), doi:10.1103/PhysRev.128.606.
- 391 [2] P. Franken, A. Hill, C. Peters, G. Weinreich, *Generation of Optical Harmonics*, Phys.  
392 Rev. Lett. **7**, 118 (1961), doi:10.1103/PhysRevLett.7.118.
- 393 [3] M. F. Ciappina, J. A. Perez-Hernandez, M. Lewenstein, *Attosecond physics at the*  
394 *nanoscale*, Rep. Prog. Phys., **80**, 054401 (2017), doi: 10.1088/1361-6633/aa574e .
- 395 [4] X.J. Fu and T. J. Cui, *Recent progress on metamaterials: From effective medium*  
396 *model to real-time information processing system*, Prog. Quant. Electron. **67**, 100223  
397 (2019), doi:10.1016/j.pquantelec.2019.05.001.
- 398 [5] C. Andraud, and O. Maury, *Lanthanide Complexes for Nonlinear Optics: From*  
399 *Fundamental Aspects to Applications*, Eur. J. Inorg. Chem., **29**, 4537(2009),  
400 doi:10.1002/ejic.200900534.
- 401 [6] S.H. Yue, M.N. Slipchenko, and J. X. Cheng, *Multimodal nonlinear optical mi-*  
402 *croscopy*, Laser Photon Rev. **5**, 496 (2011), doi:10.1002/lpor.201000027.
- 403 [7] G.F Combes, A.M. Vuckovic, K. Trajkovic, *Nanotechnology in Tumor Biomarker*  
404 *Detection: The Potential of Liganded Nanoclusters as Nonlinear Optical Con-*  
405 *trast Agents for Molecular Diagnostics of Cancer*, Cancers bf 13, 4206 (2021),  
406 doi:10.3390/cancers13164206.
- 407 [8] Y. Miyazaki and K. Kudo, in *Nonlinear Optics*, Elsevier (1992).
- 408 [9] S. Liu, P. P. Vabishchevich, I. Brener, *An all-dielectric metasurface as a broadband*  
409 *optical frequency mixer*, Nature Communications **9**, 2507 (2018), doi:10.1038/s41467-  
410 018-04944-9.
- 411 [10] Y. R. Shen, *Surface Nonlinear Optics*, J. Opt. Soc. Am. B **28**, A56 (2011), doi:  
412 10.1364/JOSAB.28.000A56
- 413 [11] Y. R. Shen, *Basic Theory of Surface Sum-Frequency Generation*, J. Phys. Chem. C  
414 **116**, 15505 (2012), doi:10.1021/jp305539v.



- 415 [12] See e.g. *Epioptics: Linear and Nonlinear Optical Spectroscopy of Surfaces and Inter-*  
416 *faces*, J. F. McGlip, D. Weaire, and C. H. Patterson eds., Springer (1995).
- 417 [13] C. Attacalite, D. Sangalli, M. Grüning, *Non-linear response of solids and nanostruc-*  
418 *tures: A real-time prospective* 2022, pp.N°154 hal-03622296.
- 419 [14] E. Luppi, H. Hübener, and V. Véniard, *Ab initio second-order nonlinear optics*  
420 *in solids: Second-harmonic generation spectroscopy from time-dependent density-*  
421 *functional theory*, Phys. Rev. B **82**, 235201 (2010), doi:10.1103/PhysRevB.82.235201.
- 422 [15] S. Hughes, *Breakdown of the Area Theorem: Carrier-Wave Rabi Flop-*  
423 *ping of Femtosecond Optical Pulses*, Phys. Rev. Lett. **81**, 3363 (1998),  
424 doi:10.1103/PhysRevLett.81.3363.
- 425 [16] A. Babaze, R. Esteban, J. Aizpurua, and A. G. Borisov, *Second-Harmonic Generation*  
426 *from a Quantum Emitter Coupled to a Metallic Nanoantenna* ACS Photonics **7**, 701  
427 (2020), doi:10.1021/acsp Photonics.9b01569.
- 428 [17] C. Attacalite, and M. Grüning, *Nonlinear optics from an ab initio ap-*  
429 *proach by means of the dynamical Berry phase: Application to second- and*  
430 *third-harmonic generation in semiconductors*, Phys. Rev. B **88**, 235113 (2013),  
431 doi:10.1103/PhysRevB.88.235113.
- 432 [18] Chao Yu, Shicheng Jiang and Ruifeng Lu, *High order harmonic generation in solids:*  
433 *a review on recent numerical methods*, Advances in Physics: X, 4:1, 1562982 (2019),  
434 DOI: 10.1080/23746149.2018.1562982
- 435 [19] N. Tancogne-Dejean, O.D. Mücke, F.X. Kärtner, A Rubio *Impact of the electronic*  
436 *band structure in high-harmonic generation spectra of solids*, Phys. Rev. Lett. **118**,  
437 087403 (2017), doi: 10.1103/PhysRevLett.118.087403.
- 438 [20] M. Orszag , P. Carrazana, and H. Chuaqui, *Quantum Theory of Second-harmonic*  
439 *Generation*, Optica Acta: International Journal of Optics, **30**, 259 (1983),  
440 doi:10.1080/713821173.
- 441 [21] G. Chesi, M. M. Wauters, N. Fasola, A. Allevi, and M. Bondani, *Second Har-*  
442 *monic Revisited: An Analytic Quantum Approach*, Applied Sciences **9**, 1690 (2019),  
443 doi:doi.org/10.3390/app9081690.
- 444 [22] M. Cini, A. D'Andrea, and C. Verdozzi, Many-photon effects in inelastic light scat-  
445 tering, Phys. Lett. A **180**, 430 (1993), doi:10.1016/0375-9601(93)90294-A.
- 446 [23] M. Cini, A. D'Andrea, and C. Verdozzi, Many-photon effects in inelastic light scat-  
447 tering: Theory and model applications, Int. Jour. Mod. Phys. **B9**, 1185 (1995),  
448 doi:10.1142/S0217979295000501.
- 449 [24] G. D. Camacho, E. Z. Casalengua, J. C. L. Carreño, S. Khalid, C. Tejedor, E. del  
450 Valle and F. P. Laussy, *Multiphoton Emission*, or arXiv:2109.12049v2 (2021).
- 451 [25] E. T. Jaynes and F. W. Cummings, Proc. *Comparison of quantum and semiclas-*  
452 *sical radiation theories with application to the beam maser*, IEEE **51**, 89 (1963),  
453 doi:10.1109/PROC.1963.1664.
- 454 [26] H. J. Carmichael and D. F. Walls, *A quantum-mechanical master equation treat-*  
455 *ment of the dynamical Stark effect*, J. Phys. B **9**, 1199 (1976), doi:10.1088/0022-  
456 3700/9/8/007.

- 457 [27] Bruce W. Shore and Peter L. Knight, *The Jaynes-Cummings Model*, *Journal of Mod-*  
458 *ern Optics*, **40**, 1195 (1993), DOI: 10.1080/09500349314551321.
- 459 [28] K. Fujii, *Dynamics of an N-level system of atoms interacting with laser fields*, *J.*  
460 *Math. Sci.*, **153**, 57 (2008), doi:10.1007/s10958-008-9120-5.
- 461 [29] Q. Xie, H. Zhong, M. T. Batchelor and C. Lee, *J. Phys. A: Math. Theor.* **50**, 113001  
462 (2017), doi:10.1088/1751-8121/aa5a65.
- 463 [30] E. Perfetto and G. Stefanucci, *Some exact properties of the nonequilibrium re-*  
464 *sponse function for transient photoabsorption*, *Phys. Rev. A* **91**, 033416 (2015),  
465 doi:10.1103/PhysRevA.91.033416.
- 466 [31] C. O'Brien and M. O. Scully, *J. Mod. Opt.*, **63**, 27 (2015),  
467 doi:10.1080/09500340.2015.1066457.
- 468 [32] *Semi-classical and quantum Rabi models: in celebration of 80 years*, *J. Phys. A: Math.*  
469 *Theor.* (2017), doi:10.1088/1751-8113/49/30/300301.
- 470 [33] W. P. Schleich, *Quantum optics in phase space* (Wiley-VCH, Berlin, 2001),  
471 doi:10.1002/3527602976.
- 472 [34] C. Cohen-Tannoudji and D. Guéry-Odelin, *Advances in atomic physics: An overview*,  
473 (World Scientific 2011), doi:doi.org/10.1142/6631.
- 474 [35] H. Walther, B. T. H. Varcoe, B.-G. Englert and T. Becker, *Cavity quantum electro-*  
475 *dynamics* *Rep. Prog. Phys.* **69**, 1325 (2006), doi:10.1088/0034-4885/69/5/R02.
- 476 [36] G. Scala, K. Słowik, P. Facchi, S. Pascazio, and F. V. Pepe, *Beyond the Rabi model:*  
477 *Light interactions with polar atomic systems in a cavity*, *Phys. Rev. A* **104**, 013722  
478 (2021), doi:10.1103/PhysRevA.104.013722.
- 479 [37] E. Boström, A. D'Andrea, M. Cini, and C. Verdozzi, *Time-resolved multiphoton*  
480 *effects in the fluorescence spectra of two-level systems at rest and in motion* *Phys.*  
481 *Rev. A* **102**, 013719 (2020), doi:10.1103/PhysRevA.102.013719.
- 482 [38] T. Hansen, S. V. B. Jensen, and L. B. Madsen *Correlation effects in high-*  
483 *order harmonic generation from finite systems*, *Phys. Rev. A* **105**, 053118 (2022),  
484 doi:10.1103/PhysRevA.105.053118.
- 485 [39] Houk Jang, Krishna P. Dhakal, Kyung-Il Joo, Won Seok Yun, Sachin M. Shinde, Xi-  
486 ang Chen, Soon Moon Jeong, Suk Woo Lee, Zonghoon Lee, JaeDong Lee, Jong-Hyun  
487 Ahn, and Hyunmin Kim, , *Transient SHG Imaging on Ultrafast Carrier Dynamics*  
488 *of MoS<sub>2</sub> Nanosheets*, *Adv. Mater.* **30**, 1705190 (2018), doi:10.1002/adma.201705190.
- 489 [40] A. Tóth, A. Csehi, G. J. Halász, and Á. Vibók, *Control of photodissociation with the*  
490 *dynamic Stark effect induced by THz pulses*, *Phys. Rev. Research* **2**, 013338 (2020),  
491 doi:10.1103/PhysRevResearch.2.013338.
- 492 [41] F. Liu, *Self-consistent tight-binding method*, *Phys. Rev. B* **52**, 10677 (1995),  
493 doi:10.1103/PhysRevB.52.10677.
- 494 [42] A. N. Andriotis and M. Menon, *Tight-binding molecular-dynamics study of ferromag-*  
495 *netic clusters*, *Phys. Rev. B* **57**, 10069 (1998), doi:10.1103/PhysRevB.57.10069.
- 496 [43] Y. Xie and J. A. Blackman, *Tight-binding model for transition metals: From cluster*  
497 *to solid*, *Phys. Rev. B* **63**, 125105 (2001), doi:10.1103/PhysRevB.63.125105.

- 498 [44] E. Boström, A. Mikkelsen, and C. Verdozzi, *Time-resolved spectroscopy at surfaces*  
499 *and adsorbate dynamics: Insights from a model-system approach*, Phys. Rev. B **93**,  
500 195416 (2016), doi:10.1103/PhysRevB.93.195416.
- 501 [45] This is of no consequence for a rigid molecule, but can have a role in general. We  
502 are currently developing a semiclassical description of the interaction between cavity  
503 modes and nuclear charge and include its effect on the motion of the nuclei.
- 504 [46] A different prescription could be to consider, irrespective of the value of  $U$ , an incident  
505 frequency in resonance with the one particle levels i.e.  $\omega_0 = 2|V_{eff}|$ . Within the  
506 perspective adopted here, this would simply amount to have an off-resonant incident  
507 field, with detuning  $\pm|2V_{eff} - \Omega_R|$ .
- 508 [47] Even with  $\beta = 3$ , the size of the incident photon subspace  $N_i$  must be much larger  
509 (explicitly,  $N_i = 60$ ) to have good numerical convergence.
- 510 [48] A.O Caldeira and A.J Leggett *Quantum tunnelling in a dissipative system*, Annals of  
511 Physics **149** 374-456 (1983), doi:10.1016/0003-4916(83)90202-6.
- 512 [49] V. Venkataraman, A. D. K. Plato, T. Tufarelli and M. S. Kim, *Affecting non-*  
513 *Markovian behaviour by changing bath structures*, J. Phys. B: At. Mol. Opt. Phys.  
514 **47**, 015501 (2014), doi:10.1088/0953-4075/47/1/015501.
- 515 [50] H. Grabert and M. Thorwart, *Quantum mechanical response to a driven Caldeira-*  
516 *Leggett bath* Phys. Rev. E **98**, 012122 (2018), doi:10.1103/PhysRevE.98.012122.
- 517 [51] J. Rogel-Salazar, *The Gross-Pitaevskii equation and Bose-Einstein condensates*, Eur.  
518 J. Phys. **34**, 247 (2013), doi:10.1088/0143-0807/34/2/247.
- 519 [52] See e.g D. Karlsson, R. van Leeuwen, Y. Pavlyukh, E. Perfetto, and G. Stefanucci,  
520 *Fast Green's Function Method for Ultrafast Electron-Boson Dynamics* Phys. Rev.  
521 Lett. **127**, 036402 (2021), doi: 10.1103/PhysRevLett.127.036402.